

Photonic-based integrated sources and antenna arrays for broadband wireless links in terahertz communications

E García-Muñoz¹, K A Abdalmalak¹ , G Santamaría¹, A Rivera-Lavado¹ ,
D Segovia-Vargas¹, P Castillo-Aranibar², F Van Dijk³, T Nagatsuma⁴,
E R Brown⁵, R C Guzman⁶, H Lamela⁶ and G Carpintero⁶ 

¹Departamento de Teoría de Señal y Comunicaciones, Universidad Carlos III de Madrid, Leganés (Madrid), Spain

²Universidad Católica San Pablo, Arequipa, 04001 Peru

³III-V Laboratory, Palaiseau, F-91767, France

⁴Graduate School of Engineering Science, Osaka University, Toyonaka (Osaka), Japan

⁵Department of Electrical Engineering, Wright State University, Dayton (Ohio), United States of America

⁶Departamento de Tecnología Electrónica, Universidad Carlos III de Madrid, Leganés (Madrid), Spain

E-mail: guiller@ing.uc3m.es

Received 12 August 2018, revised 2 November 2018

Accepted for publication 17 December 2018

Published 29 March 2019



CrossMark

Abstract

This paper analyzes integrated components for ultra-broadband millimeter-wave wireless transmitters enabling the 5 G objective to increase the wireless data rates $10\times$ to $100\times$. We have pursued the photonic-based approach to generate the millimeter-wave carrier (≈ 97 GHz in this paper) through photomixing. We have achieved up to 10 Gb s^{-1} data rate using an OOK modulation format (to reduce latency) and either direct detection (DD) or coherent detection. We show that coherent detection enables a sensitivity improvement of 17 dB over DD. We also demonstrate in this work that such improvement can be achieved using as the transmitter a novel integrated antenna array—the self-complementary chessboard array. This avoids the use of complex coherent schemes at the receiver, enabling simple DD for ultra-broadband links.

Keywords: photonic integration, photomixing, direct detection, coherent detection, wireless links, millimeter-wave, antenna arrays

(Some figures may appear in colour only in the online journal)

1. Introduction

One of the motivations behind the development of 5 G is to reduce the latency and increase the bandwidth of wireless communication links up to 100 Gb s^{-1} in order to enable a seamless integration of wired and wireless communication links [1]. This is particularly required for point-to-point links connecting to the network over a range of densely distributed wireless pico-cells positioned closer to the end user to

enhance the mobile broadband performance in areas with high traffic [2]. In order to reduce the latency, the modulation schemes should be as simple as possible, On–Off Keying being the extreme case. This is not possible at microwave frequencies simply because there is no spectrum allocation that can provide the required bandwidth. So the carrier frequencies have been pushed up to the millimeter-wave (MMW, 30–300 GHz) and terahertz (THz, 0.3–3 THz) ranges [3]. For example, recent experiments demonstrated data rates up to 48 Gb s^{-1} on a 300 GHz carrier frequency [3]. One of the bottlenecks for these systems is the generation of carriers at these frequencies having satisfactory power and signal quality. Photonic-based generation requires a laser source and an ultrafast photodiode (or photoconductive device). The



Original content from this work may be used under the terms of the [Creative Commons Attribution 3.0 licence](https://creativecommons.org/licenses/by/3.0/). Any further distribution of this work must maintain attribution to the author(s) and the title of the work, journal citation and DOI.

optical source depends on the photonic technique used to generate the MMW or THz frequencies, the two most common being cw photomixing and pulsed photoconductive switching.

Pulsed sources generally utilize a mode locked laser (MLL) [4] and have two major advantages over cw techniques. The first advantage is ~ 7 dB higher average power levels than photomixing schemes [5]. The second is that MLLs inherently have very stable pulse repetition frequency (PRF) and low pulse-to-pulse jitter [6]. However, MLLs have one major disadvantage: the PRF is fixed by the laser resonator cavity length so cannot be modulated. Therefore, photomixing is the preferred technique when frequency tuning is desired. It requires a laser (or lasers) having two different optical wavelengths, the simplest approach being separated distributed feedback (DFB) lasers. These optical wavelengths are mixed in the photodiode or photoconductive device, generating an electrical beat-note at the difference frequency. Its main drawback is that when the two wavelengths are generated from independent sources, the beat-note exhibits large phase-noise fluctuations associated with the linewidth of the lasers and to the relative wavelength fluctuation between them.

This problem can be addressed using different approaches. The most common has been to stabilize the wavelengths using optical injection or optical phase-locked loops [7]. More recently, the monolithic integration of two DFBs side-by-side has improved the stability by having the two lasers experience the same environmental conditions. Using long quantum-dash cavities and combining the wavelengths using a Y-junction, researchers have demonstrated tuning ranges from 2 to 20 GHz and optical line widths around 1 MHz [8].

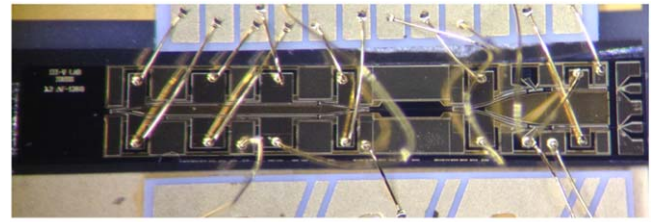
Finally, in order to increase the transmit power level, a novel integrated array has been developed and is reported here for the first time. It is based on a planar array of photomixers, each coupled to a self-complementary antenna. We call this new transmitter approach the ‘chessboard’ array.

The paper is organized as follows. The following section, section 2, presents the radio link powered by an integrated photonic source, section 3 describes the chessboard array to increase the power level, and section 4, presents the conclusion.

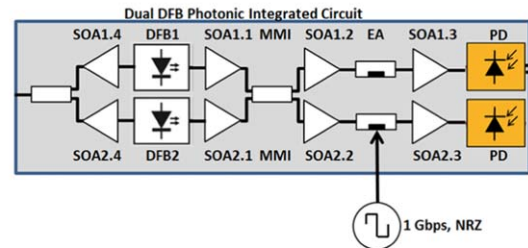
2. Photonic integrated optical heterodyne source

Figure 1 shows the block diagram and a photograph of the fabricated photonic integrated circuit (PIC) dual-wavelength laser source designed for the MMW range [9].

For the present purposes, we use only the left-hand side of the chip including two single-mode, 1 mm long DFB lasers combined into a single output waveguide with a 2×1 multimode interference (MMI) coupler. This optical port provides an optical output for the dual-wavelength lasers and is designed to allow phase noise reduction through optical injection locking [10]. This chip is especially suited for photomixing, being grown on a semi-insulating InP wafer in order to reduce the parasitic capacitance using butt-joint



(a)

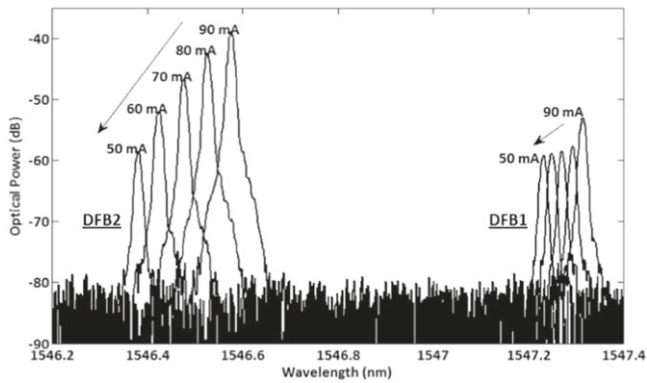


(b)

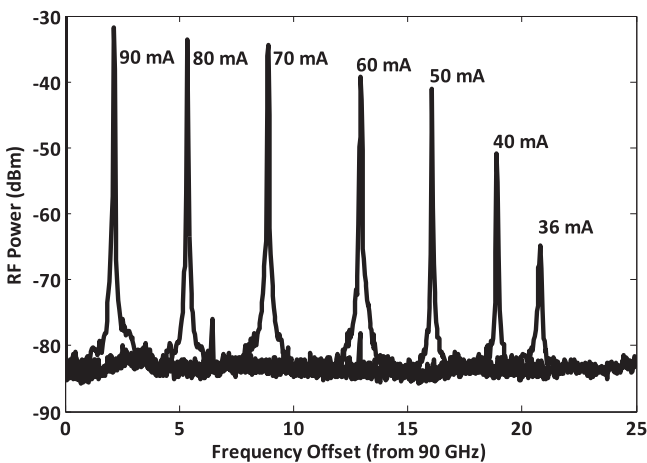
Figure 1. (a) Picture of the fully integrated dual wavelength source for millimeter wave generation. (b) Block diagram of the integrated elements.

active/passive integration. The active layers consist of 6 InGaAsP quantum wells, and are the same for the DFB lasers, the semiconductor optical amplifiers (SOAs) and electro-absorption modulation sections. As the DFB emission wavelength and power both vary with the injection current, the SOAs are utilized to equalize the optical power after the MMI.

The wavelength of each of the DFB lasers on this PIC can be continuously tuned varying their injection current [11], which allows varying the generated beat-note frequency. This characteristic is demonstrated in the optical domain in figure 2(a). While maintaining DFB1 current level fixed at 75 mA, the current injected in DFB2 is varied between 50 and 90 mA in 10 mA current steps. At the initial current combination (DFB1 = 75 mA, DFB2 = 50 mA), the two lasers emit the same optical output power, and the frequency spacing between their wavelengths is 105 GHz. As we increase the current level in DFB2, its wavelength shifts to longer values, getting closer to DFB1. The wavelength difference between the two DFB lasers decreases and the beat-note frequency decreases accordingly. In figure 2(b), we show the beat-note measured by probing the integrated photodiode with a WR08 waveguide output probe, followed by an F-band sub-harmonic mixer with a LO frequency of 45 GHz. The photodiode was biased at -2.5 V, so that the maximum generated photocurrent level was below 6 mA. The beat-note frequency varies from 105 to 92 GHz when the current in DFB2 is varied from 50 to 90 mA. The DFB2 wavelength change is due to the temperature increase when the injection current is increased, by thermal expansion of the DFB grating. However, the increase in DFB2 current causes two unwanted side effects. The first is due to thermal crosstalk between the two DFBs, which results in a shift of both wavelengths. The second is that increasing DFB2 current also increases its emitted optical power, causing a growing amplitude



(a)

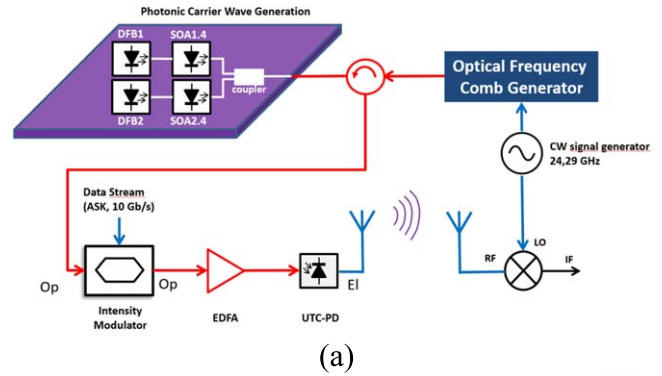


(b)

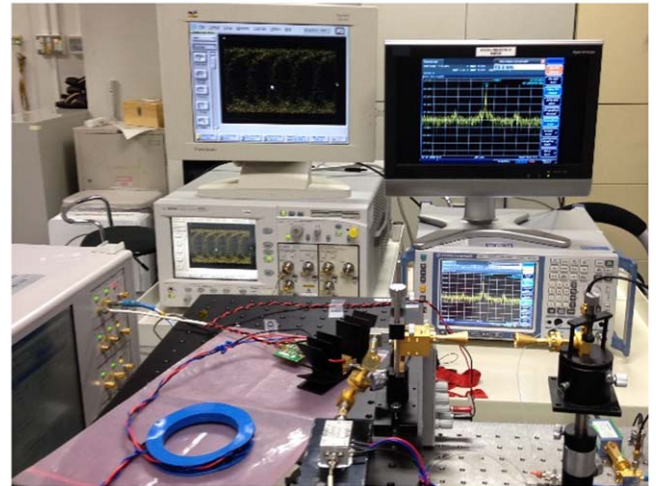
Figure 2. Dual-DFB PIC results varying the current into DFB2 (90–40 mA) for a fixed current on DFB1 (70 mA): (a) Optical spectra, (b) Beat-note spectra measured in F band, with the x-axis as the offset from 90 GHz.

difference between the two wavelengths, and increasing the DC component of the photocurrent.

The dual-wavelength laser source PIC was then included into a coherent wireless data transmission experiment, composed of the building blocks shown in figure 3(a). The function for the PIC was to provide the photonic signal to generate the millimeter-wave carrier frequency. For the coherent detection, the two lasers must be phased-locked. This is achieved through optical injection into both lasers the output from a separate optical frequency comb (OFC) generator source. This stabilizes the wavelengths of the two lasers, DFB1 and DFB1, and creates high-spectral-purity signals with phase noise spectral density below -90 dBc Hz^{-1} at 10 kHz offsets from the carrier [10]. The optical comb source signal is generated by the cascaded phase modulation of a tunable 1550 nm seed laser as previously described [3]. The frequency difference of the two DFBs was set at 97.16 GHz. A continuous-wave generator was set at the fourth subharmonic ($97.16/4 = 24.29$ GHz) and then used as an OFC generator in the transmitter as well as the LO in the receiver. An optical circulator at the output port of the PIC allowed us to separate the OFC optical injection signal from



(a)



(b)

Figure 3. (a) Building blocks of the coherent wireless data transmission using the dual DFB PIC for carrier wave generation. Only the coherent detection scheme is shown in the receiver. (b) Photograph of the experimental setup.

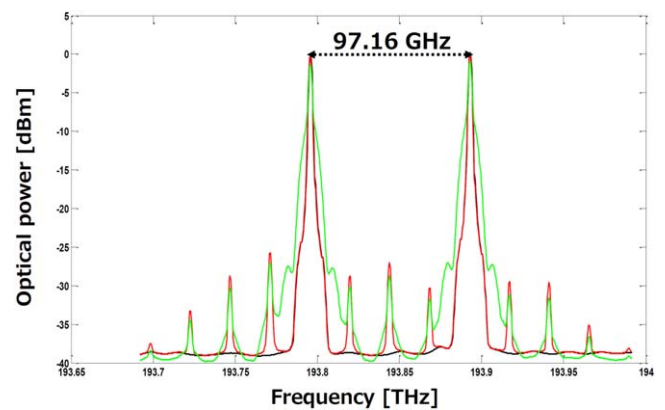


Figure 4. Optical signals in the coherent wireless transmission system: (black) the optical output from the PIC when the two DFB lasers are biased simultaneously; (red), PIC output when the OFC signal is injected; (green), output of the intensity modulator. Note that the black curve is superimposed on the red in the two wavelength peaks.

the dual-wavelength output of the PIC. A photograph of all the experimental components is shown in figure 3(b).

Figure 4 shows the most relevant optical signals in this system. The black trace shows the optical spectrum at the PIC

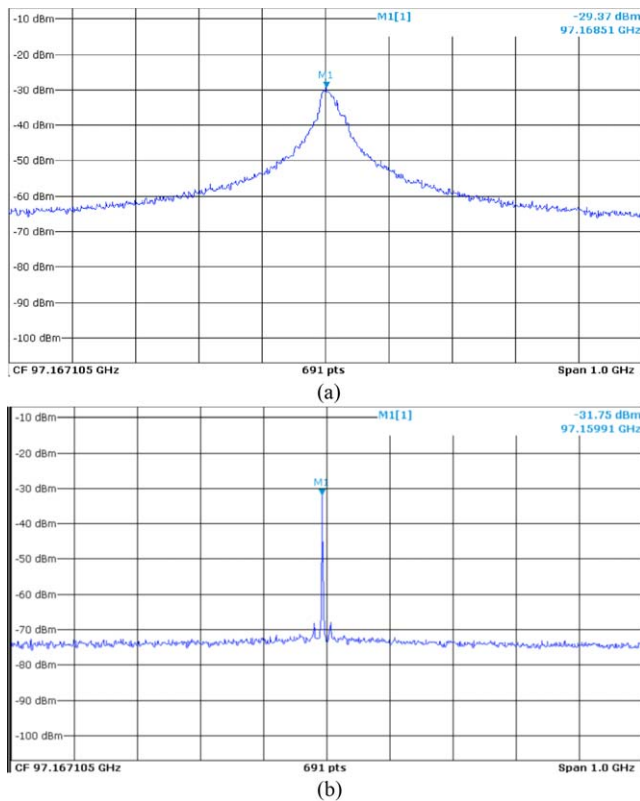


Figure 5. Beat note at 97.17 GHz, from (a) the free-running dual DFB and (b) the dual DFB under optical injection from the OFC generator.

output port when the two lasers are biased with current, and their wavelengths combined. The currents were adjusted to achieve a wavelength spacing of 97.16 GHz, and the side mode suppression ratio (SMSR) is shown to be higher than 35 dB. This is the free-running operating condition, in which the two lasers are independent oscillators with uncorrelated noise processes. In the locked operating condition (red trace), the two wavelengths are phase locked through optical injection of the OFC signal at a power of -6.2 dBm. Stray optical wavelengths from the OFC are visible, and the SMSR level is 25 dB. When this optical signal is intensity modulated, at 10 Gb/s, the optical spectrum is given by the green trace. It is shown that all the optical modes widen due to the data bandwidth. After the modulation, the optical signal was amplified with an erbium-doped fiber amplifier (EDFA). The W-band signal was generated from the EDFA output using an Uni-Traveling Carrier Photodiode (UTC-PD). The total output into free space was measured to be -23 dBm. Figure 5 shows the beat note at 97.16 GHz on a 100 kHz resolution bandwidth. The signal under free-running conditions is shown in figure 5(a), with ~ 10 MHz full-width half maximum linewidth. Figure 5(b) shows the linewidth under optical injection, when it is significantly reduced.

At the receiver side, we used two detection schemes. The first is direct detection (DD), using a quasi-optical Schottky barrier diode (VDI QOD, with 100–1000 GHz RF bandwidth and 40 GHz video bandwidth) acting as an envelope detector. The second scheme is coherent detection, using a harmonic

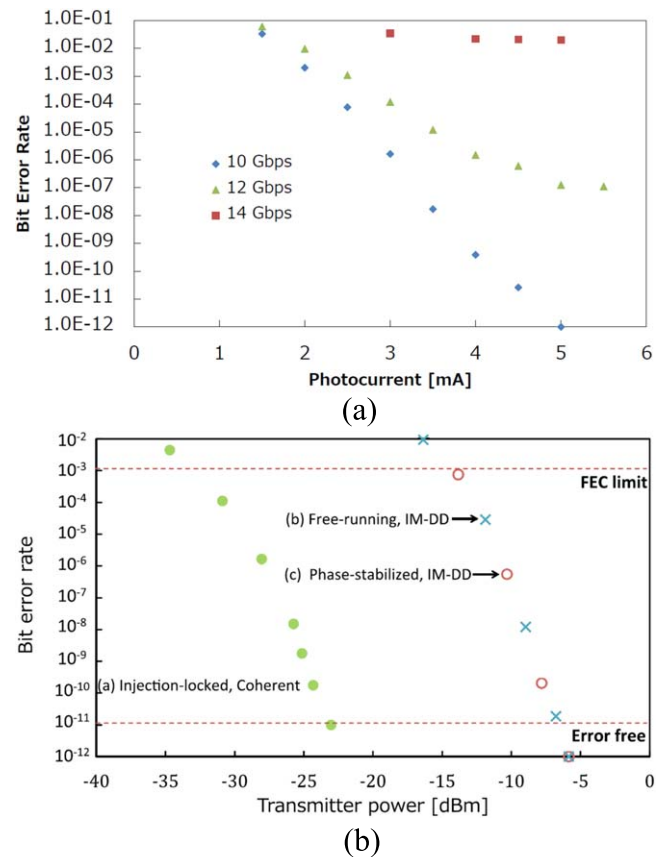


Figure 6. Bit error rate characteristics (a) phase stabilized dual DFB and direct detection, parameterized by the data rate (b) comparison between direct (free running, x, or phase-stabilized, o) versus coherent detection (injection locked, •).

mixer (VDI WR8.0ZBD, with WR08 RF input and 19.8 GHz video bandwidth), in which the use of a local oscillator (LO) signal and narrow intermediate-frequency bandwidth provides higher sensitivity.

The bit error rate was measured as a function of the radiation power under injection locked condition of the DFB lasers and coherent detection. The results are plotted in figure 6(a). We used a pseudo random ($2^{15}-1$) length bit stream which increases the bit rate from 10 to 14 Gbit s^{-1} . We observe that up to 10 Gbit s^{-1} data-rate, we are able to achieve error-free transmission ($BER < 10^{-11}$), but not with higher data rate increases. The reason is the aliasing between the modulation side-bands on both DFB sub-carriers (figure 4) caused by the OFC injection. Then we compared the BER in the locked and free-running condition (figure 6(b)) with DD, and compared those results versus the best-case scenario—DFB lasers locked with coherent detection. With DD there is no advantage of stabilizing the lasers (o points) versus using them in the free-running state (x points). The real difference is achieved when the coherent scheme is used, with error-free transmission (BER of 9.9×10^{-12}) and 17 dB sensitivity improvement over the DD. Figure 7 shows the recorded eye pattern in the error-free condition. According to Friis' formula, coherent detection thus enables about 7 times longer transmission range than DD.

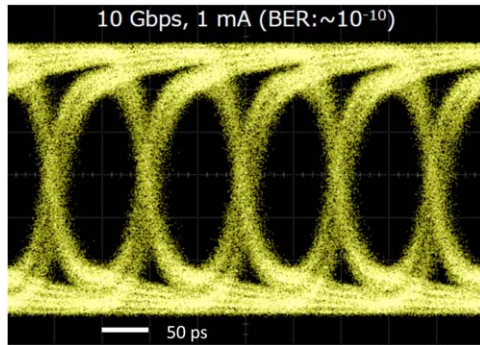


Figure 7. Eye pattern of the coherent scheme in the error-free condition.

This improvement in the sensitivity is at the cost of increasing the complexity of the transmitter (OFC) and receiver (heterodyne conversion). This has a high impact on the cost of the system. If the transmitted power were increased significantly, the simpler and cost-effective DD scheme would be enabled, avoiding the phasing issues in both transmitter and receiver sides.

3. Antenna array

The above experiment demonstrates the possibility of achieving a data rate up to 10 Gbps with an integrated photonic source. However, from figure 3(b) it can be seen that the antenna used for the link is a 20 dBi conical horn antenna that precludes a fully integrated solution and is bandwidth limited (75–110 GHz due to the single waveguide-mode configuration). Also, the transmitter as configured cannot provide a power larger than that associated with a single PIC.

To overcome these drawbacks an array configuration for increasing the emitted power is demonstrated in this section. In array configurations, the sources must have mutually coherent properties. This is possible by using the same laser sources for all photomixers. This approach was first demonstrated by Preu *et al* [12, 13]. In [13] the authors used two photomixing sources in a Young's experiment setup for measuring the coherence length. In [12], it is shown how N sources can be combined for increasing the generated THz power. An intensity improvement of N^2 is achieved in the direction of the maximum of the radiation pattern [12, 14], although the total radiated power increases only N -fold as expected from classical electromagnetics. This power increase should yield either a BER reduction at a given range, or a range enhancement at a given BER.

3.1. Experimental set-up

Figure 8 shows the side view of the proposed array approach. A Gaussian optical beam (blue) is focused on a 2D rectangular array of photomixing sources (dark-red) by using a fused silica microlens array. This preserves the illumination efficiency since it avoids delivering power to non-active areas. The generated THz signal is radiated into the InP

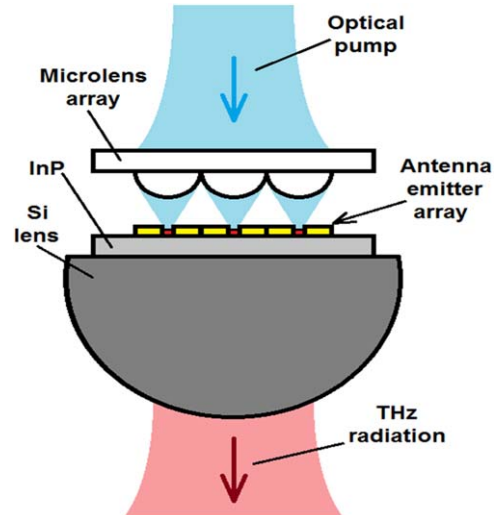


Figure 8. Sketch of the chessboard array. The optical pump (blue) is focused in the photomixing devices (dark-red) by a microlens array. The generated THz signal (light-red) is radiated into the substrate (light-gray) by bow ties antennas (gold) and, finally, into the air by using a silicon lens (dark-gray).

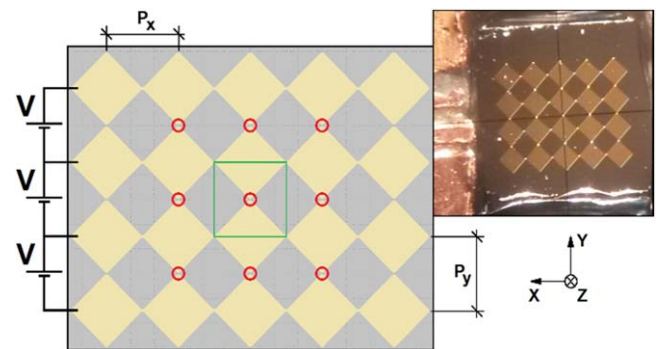


Figure 9. A 3×3 photomixers chessboard array. The devices (red) are placed in the gaps of bow tie antennas (gold) on a $300 \mu\text{m}$ center-to-center pitch. Each photomixer has an active area of $10 \times 10 \mu\text{m}^2$. The central element is marked with a green box. The inset shows a fabricated device before adding the bias connections.

substrate (light-gray) by bow tie antennas (gold). A hyper-hemispherical silicon lens (dark-gray) is placed below the substrate for radiating the THz power into the air. A detailed top-view of the 2D array configuration is shown in figure 9, showing the antenna geometry. It is based on the planar, self-complementary bowtie which can provide stable radiation patterns and behavior over the required broadband. Also, in this array configuration, the mutual coupling can be controlled. For example, the optimum pitch size between the elements has been carefully selected to be significantly less than the wavelength at the lower frequencies which will purposefully increase the mutual coupling to constructively enhance the performance at these frequencies.

The bow-tie antennas are laid out in a cartesian grid such that when rotated 45° the array resembles a 'chessboard' pattern on the InP substrate. It is also easy to see that the interconnected self-complementary structure provides an equal and constant RF impedance in all the driving ports (i.e.

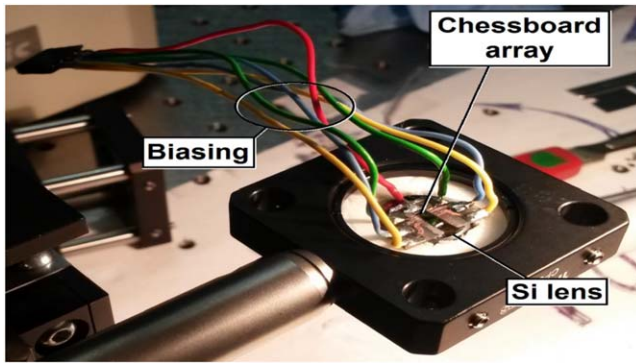


Figure 10. Assembly of the 3×3 chessboard array shown in figure 9 inset. The array is aligned and then glued onto the backside of a silicon lens. Next, a PCB for doing the bias connections is added.

photomixers). In addition, if the photomixers are mutually coherent and synchronous, there should be a stable radiation pattern in the broadband direction. Figure 9 shows a 3×3 element array with $300 \mu\text{m}$ pitch in both dimensions. Two extra rows and columns of passive antennas have been added to increase the array size and avoid truncation effects. The $300 \mu\text{m}$ pitch is quite convenient for assembly purposes [15] due to the availability of rectangular-grid microlens arrays, such as the commercial MLA300-14AR. One of the main advantages of the proposed design is the biasing set-up. Each row of the array is given the same voltage V , and the row-to-row difference is the desired photomixer bias voltage. Hence, all devices will have the same bias. Another advantage is its polarization stability in the whole band. Being very broadband and dipole-like in nature, the bowtie antennas radiate E and H plane polarizations that are nominally orthogonal with around -10 dB of cross-pol level. This orthogonal polarization could provide another benefit for a communication link by using polarization diversity.

The devices have been manufactured by HHI using not UTC-PDs but rather an ultrafast InGaAs photoconductive photomixer having an interdigitated-electrode structure. The central element of the array is aligned to the Si-lens optical axis by using a microscope with a reticle (see figure 9 inset) and a 2-axis micro-positioner having alignment precision below $\pm 10 \mu\text{m}$. The fully assembled chessboard array and bias scheme are displayed in figure 10.

The alignment of the microlens array to the input laser is the most critical step in the assembly process. It can be done by using a 5-axis mechanically controlled micro-positioner (see figure 11). By adjusting the distance between the microlens and the photomixer planes, it is possible to modify the spot sizes, which can be used to trade-off the alignment accuracy with illumination inefficiency.

3.2. Simulation results

The concept has been validated for different array sizes through full-wave simulations. The array pitch can be tailored to specific antenna sizes in order to cover different THz bands. In this Section two designs are presented, one working

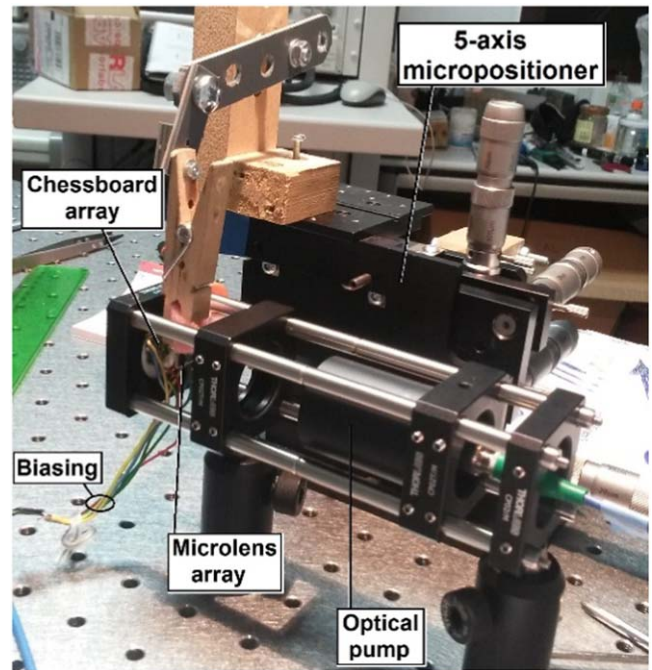


Figure 11. Full assembly. An optical system is added for controlling the laser spot size and collimation. A 5-axis micropositioner places the microlens array between the chessboard array and the laser optical system.

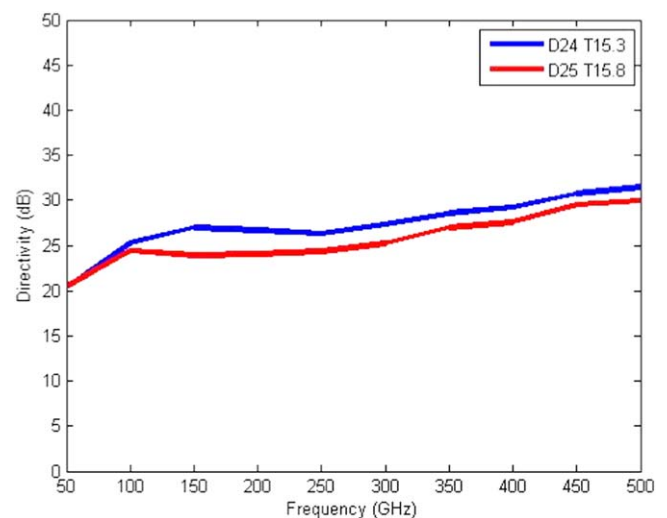


Figure 12. Simulated directivity of the chessboard array of pitch $P_x = P_y = 227 \mu\text{m}$. Two different lens designs have been considered.

up to 500 GHz and the second one working up to 2 THz. A study of each array configuration together with different Si-hyper-hemisphere designs is presented in terms of directivity. Figure 12 shows the achieved directivity for a design working up to 500 GHz. It has a pitch $P_x = P_y$ of $227 \mu\text{m}$. Two different commercial hyper-hemispherical lenses were considered for the simulation: the first one has a diameter of 24 mm and a thickness of 15.3 mm (D24, blue); and the second one has a diameter of 25 mm and a thickness of 15.8 mm (D25, red). The lowest frequency considered for this

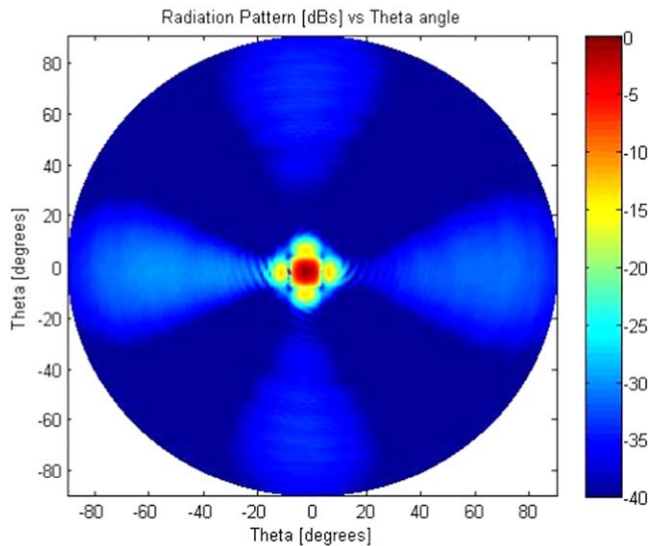


Figure 13. 2D radiation pattern of the Chessboard array of pitch $P_x = P_y = 227 \mu\text{m}$.

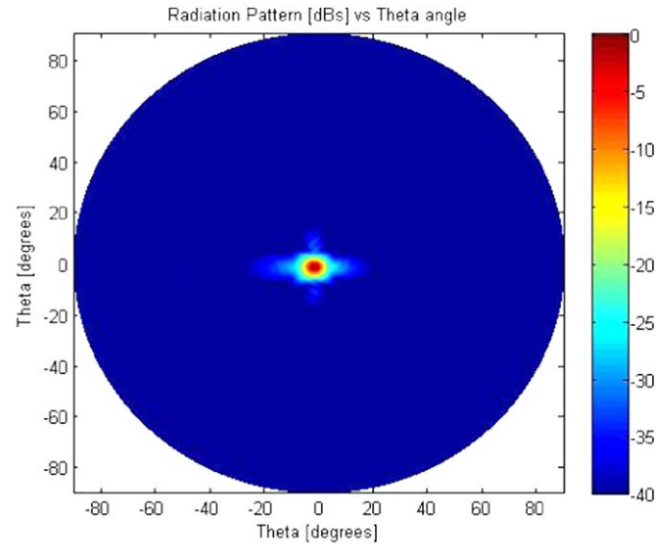


Figure 15. 2D radiation pattern of the chessboard array of pitch $P_x = P_y = 57 \mu\text{m}$.

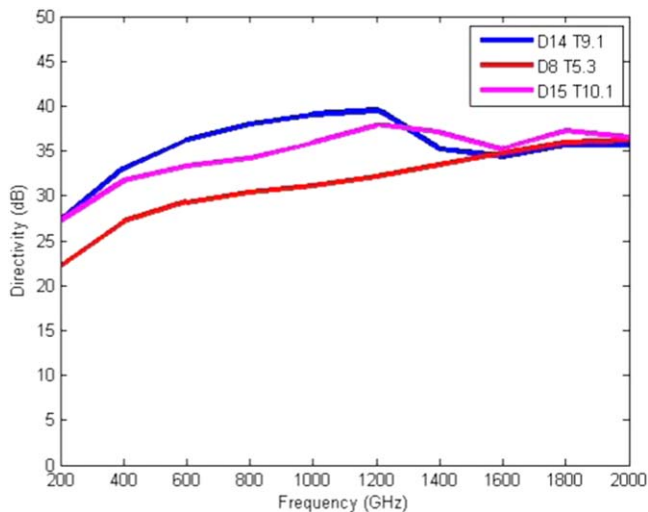


Figure 14. Simulated directivity of the chessboard array of pitch $P_x = P_y = 57 \mu\text{m}$. Three different lens designs have been considered.

design is 50 GHz. Figure 13 shows the 2D radiation pattern of the array when using the 25 mm diameter lens.

A second design was developed working up to 2 THz by reducing the pitch down to $P_x = P_y = 57 \mu\text{m}$. Its directivity (see figure 14) was obtained for three different commercial Si hyper-hemispherical lenses: a bullet lens with a diameter of 14 mm and a thickness of 9.1 mm (D14 T9.1, blue); a bullet lens with a diameter of 8 mm and a thickness of 5.3 mm (D8 T5.3, red); and a wider lens with a diameter of 15 mm and a thickness of 10.1 mm (D15 T10.13, pink). Figure 14 compares the directivity of all three in the 200–2000 GHz frequency band. figure 15 displays the 2D radiation pattern for the (D8 T5.3, red) bullet lens.

The THz emitted power has been measured for the second design with first lens (14 mm diam bullet lens) up to 500 GHz (figure 16) The radiated cw power in the

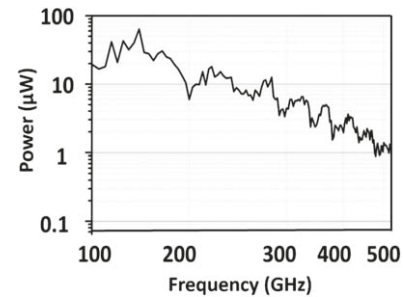


Figure 16. Measured THz emitted power (μW) versus frequency for the first array design.

100–200 GHz band has been measured with a 13 Hz chopped Golay cell having a filter to block IR but pass THz, and a lock-in amplifier for synchronous demodulation. The maximum radiated cw power was approximately 40–50 μW at frequencies around 150 GHz. This is 8–10 times greater than that of the UTC-PD near 97 GHz in the above communications demonstration. In addition, the chessboard array enables a modular transmitter where the DFB lasers and modulation components are integrated into one PIC, and the photomixers are integrated into a separate monolithic chip. The improvement in power made possible by the chessboard array will allow us to realize, according to figure 6, excellent communications-link performance using a simple DD receiver, and even better performance if a coherent receiver is justified.

4. Conclusions

In this paper we present key advancements for the deployment of 5 G wireless systems. On one hand, we demonstrate a PIC for generation, optical-frequency-comb stabilization, and modulation of carrier waves in the millimeter-wave range (W-band) through photomixing. This technique enables the seamless integration of wired and wireless links. Error-free

real time data transmission at 10 Gb s^{-1} is achieved for direct and coherent detection. The direct-detection data rate was limited only by the frequency spacing of the OFC. Coherent detection enabled a sensitivity improvement of about 17 dB, but at the expense of significantly increased receiver complexity. Direct detection can be maintained through an increase of the transmitted power. To this end, we have also presented a novel photomixing power-combining scheme—the chessboard array. Since the number of elements can be increased with no extra assembly complexity, the chessboard array can potentially become an appealing high-power optoelectronic terahertz cw coherent source for many applications besides communications.

Acknowledgments

The authors acknowledge Dr David González Ovejero for fruitful discussions on antenna simulation. This work has been financially supported by Ministerio de Economía, Industria y Competitividad iTWIT Project with references TEC2016-76 997-C3-2-R and TEC2016-76 997-C3-3-R. Authors also acknowledge Ayuda Fundación BBVA a Investigadores y Creadores Culturales 2016' and 'Estancias de movilidad de profesores PRX16/00 021'.

ORCID iDs

K A Abdalmalak  <https://orcid.org/0000-0002-9544-2412>
 A Rivera-Lavado  <https://orcid.org/0000-0002-4684-3949>
 G Carpintero  <https://orcid.org/0000-0001-6665-3977>

References

- [1] Nagatsuma T and Carpintero G 2015 Recent progress and future prospect of photonics-enabled terahertz communications research *IEICE Trans. Electron.* **E98-C** 1060–70
- [2] Fixed networks for mobile backhaul' Application note, Nokia 2016
- [3] Nagatsuma T, Horiguchi S, Minamikata Y, Yoshimizu Y, Hisatake S, Kuwano S, Yoshimoto N, Terada J and Takahashi H 2013 Terahertz wireless communications based on photonics technologies *Opt. Exp.* **21** 23736–47
- [4] Nagatsuma T, Hirata A, Shimizu N, Song H J and Kukutsu N 2007 Photonic generation of millimeter and terahertz waves and its applications *Appl. Electromagn. Commun. ICECom (Dubrovnik, Croatia)* (IEEE) 1–4
- [5] Moeller L, Shen A, Caillaud C and Achouche M 2013 Enhanced THz generation for wireless communications using short optical pulses *Infrared, Millim. Terahertz Waves (IRMMW-THz) (Mainz, Germany)* (IEEE) 1–3
- [6] Carpintero G, Thompson M G, Pentyl R V and White I H 2009 Low noise performance of passively mode-locked 10-GHz quantum-dot laser diode *IEEE Photonics Tech. Lett.* **21** 389–91
- [7] Johansson L A and Seeds A J 2003 Generation and transmission of millimeter-wave data-modulated optical signals using an optical injection phase-lock loop *J. Light. Tech.* **21** 511–20
- [8] Van-Dijk F, Accard A, Enard A, Drisse O, Make D and Lelarge F 2011 Monolithic dual wavelength DFB lasers for narrow linewidth heterodyne beat-note generation *Int. Topical Meeting on Microwave Photonics 2011* pp 73–6
- [9] van Dijk F et al 2014 Monolithically integrated InP Heterodyne millimeter wave source for high data rate transmission *IEEE Photonics Tech. Lett.* **26** 965–8
- [10] Balakier K, Fice M J, van Dijk F, Kervella G, Carpintero G, Seeds A J and Renaud C C 2014 Optical injection locking of monolithically integrated photonic source for generation of high purity signals above 100 GHz *Opt. Express* **22** 29404–12
- [11] Carpintero G, Guzmán R C, Gordón C, Kervella G, Chitoui M and Van Dijk F 2016 Photonic integrated circuits for radio-frequency signal generation *J. Light. Tech.* **34** 508–15
- [12] Preu S, Malzer S, Döhler G, Zhang J, Lu Z and Wang L 2006 Highly collimated and directional continuous-wave terahertz emission by photomixing in semiconductor device arrays *Proc. SPIE* **6194** 61940F
- [13] Preu S, Malzer S, Döhler G, Zhao Q, Hanson M, Zimmerman J, Gossard A and Wang L 2008 Interference between two coherently driven monochromatic terahertz sources *Appl. Phys. Lett.* **92** 221107
- [14] Döhler G, García-Muñoz L E, Preu S, Malzer S, Bauerschmidt S, Montero-de-Paz J, Ugarte-Munoz E, Rivera-Lavado A, Gonzalez-Posadas V and Segovia-Vargas D 2013 From arrays of THz antennas to large-area emitters *IEEE Trans. Terahertz Sci. Technol.* **3** 532–44
- [15] Sartorius B, Stanze D, Göbel T, Schmidt D and Schell M 2012 Continuous wave terahertz systems based on 1.5 μm telecom technologies *J. Infrared, Millim. Terahertz Waves* **33** 405–17